LETTERS

Tunable delay of Einstein–Podolsky–Rosen entanglement

A. M. Marino[1], R. C. Pooser[1], V. Boyer[1,2] & P. D. Lett[1]

Entangled systems display correlations that are stronger than can be obtained classically. This makes entanglement an essential resource for a number of applications, such as quantum information processing, quantum computing and quantum communications[1,2]. The ability to control the transfer of entanglement between different locations will play a key role in these quantum protocols and enable quantum networks[3]. Such a transfer requires a system that can delay quantum correlations without significant degradation, effectively acting as a short-term quantum memory. An important benchmark for such systems is the ability to delay Einstein–Podolsky–Rosen (EPR) levels of entanglement and to be able to tune the delay. EPR entanglement is the basis for a number of quantum protocols, allowing the remote inference of the properties of one system (to better than its standard quantum limit) through measurements on the other correlated system. Here we show that a four-wave mixing process based on a double-lambda scheme in hot ^{85}Rb vapour allows us to obtain an optically tunable delay for EPR entangled beams of light. A significant maximum delay, of the order of the width of the cross-correlation function, is achieved. The four-wave mixing also preserves the quantum spatial correlations of the entangled beams. We take advantage of this property to delay entangled images, making this the first step towards a quantum memory for images[4].

The implementation of a quantum protocol usually requires the transfer of entanglement between different locations of the quantum processor to be properly synchronized. This requires tunable delays at least as large as the inverse of the maximum bandwidth of the signal (in our case given by the width of the cross-correlation function), that is to say, large tunable fractional delays. In general, applications such as quantum information processing and computing will require fractional delays larger than one, while quantum communications between distant locations will require much larger fractional delays. Light provides an excellent means to achieve this goal, as its propagation velocity can be controlled by tailoring the optical response of the medium. Indeed, a positive change of the index of refraction as a function of frequency leads to a reduced group velocity over a frequency range. For instance, the narrow transparency window obtained with electromagnetically induced transparency[5], the transparent region between two absorption resonances[6], or the sharp gain feature obtained with four-wave mixing in a double-lambda system[7], all lead to a large dispersion over a small frequency range and a large reduction in group velocity.

Up to now, breakthroughs in the areas of delay and storage of quantum states have been achieved in the single photon regime, for which quantum delay lines[8] and quantum memories[9–11] have been demonstrated. Continuous variables, such as the amplitude and phase of a beam of light, offer the possibility of generating entanglement deterministically, can be measured with high efficiency, and can be efficiently mapped onto atomic ensembles. These properties are crucial for the efficient implementation of a number of quantum information protocols[2] and make deterministic continuous-variable systems an attractive alternative to single photon systems. In the continuous-variable regime, results have been limited to the delay[12] and storage[13,14] of the squeezing properties of a single-mode beam of light and more recently to a small fractional delay (the ratio of the delay to the full-width at half-maximum of the cross-correlation function between the entangled beams after the delay) of the order of 0.08 for entanglement in the form of inseparability[15]. These experiments have been based on electromagnetically induced transparency, which has limited the storage efficiencies to values of the order of 15–20% (refs 13, 14). This poses an important constraint on the use of this process as a delay mechanism or quantum memory for continuous-variable entanglement. Here we show that four-wave mixing offers an alternative that preserves continuous-variable entanglement at the EPR level over a significant fractional delay and has the possibility of acting as a multi-spatial-mode delay line, allowing us to delay entangled images.

In order to characterize the entanglement between two systems, a and b, we need to analyse joint variables. For the case of the electromagnetic field, these variables correspond to the joint quadrature operators $\hat{X}_- = (\hat{X}_a - g\hat{X}_b)/\sqrt{2}$ and $\hat{Y}_+ = (\hat{Y}_a + g\hat{Y}_b)/\sqrt{2}$, which combine the amplitude $(\hat{X}_a, \hat{X}_b)$ and phase $(\hat{Y}_a, \hat{Y}_b)$ quadratures of the two systems. Here, g is a scaling factor which is adjusted to optimize the different entanglement criteria. Physically, the joint quadratures correspond to the amplitude difference, $\hat{X}_-$, and phase sum, $\hat{Y}_+$, between the fields for $g = 1$. Based on the noise properties of these quadratures, different degrees of continuous-variable entanglement exist. The variance, or noise, of these operators for coherent states sets the standard quantum limit (SQL) of the quadrature fluctuations. The minimum requirement for entanglement is that the states of the two systems cannot be described independently, a property known as inseparability. This property can be quantified with the inseparability parameter $\mathcal{I} = \langle \Delta\hat{X}_-^2 \rangle_N + \langle \Delta\hat{Y}_+^2 \rangle_N$, where the N subscript indicates that the variances have been normalized to the corresponding SQL. The state of the system is inseparable when $\mathcal{I} < 2$ for some value of g (ref. 16), such that having both $\langle \Delta\hat{X}_-^2 \rangle$ and $\langle \Delta\hat{Y}_+^2 \rangle$ below the SQL, or squeezed, for some g is a sufficient condition for entanglement. A stronger degree of quantum correlation is given by EPR entanglement, which can be quantified with the conditional variances of system a given system b, $V_{X_a|X_b}$ and $V_{Y_a|Y_b}$. We can define the EPR parameter $\mathcal{E}_{ab} = V_{X_a|X_b} \cdot V_{Y_a|Y_b}$ such that $\mathcal{E}_{ab} < 1$ indicates the presence of EPR entanglement[17]. In practice, it is not necessary to measure the conditional variances directly as they can be derived from the joint quadratures, as discussed in the Supplementary Information.

The experiment uses four-wave mixing in a double-lambda configuration (Fig. 1 inset), in two separate ^{85}Rb cells, to first generate[18,19]

[1]Joint Quantum Institute, National Institute of Standards and Technology and University of Maryland, Gaithersburg, Maryland 20899, USA. [2]MUARC, School of Physics and Astronomy, University of Birmingham, Edgbaston, Birmingham B15 2TT, UK.

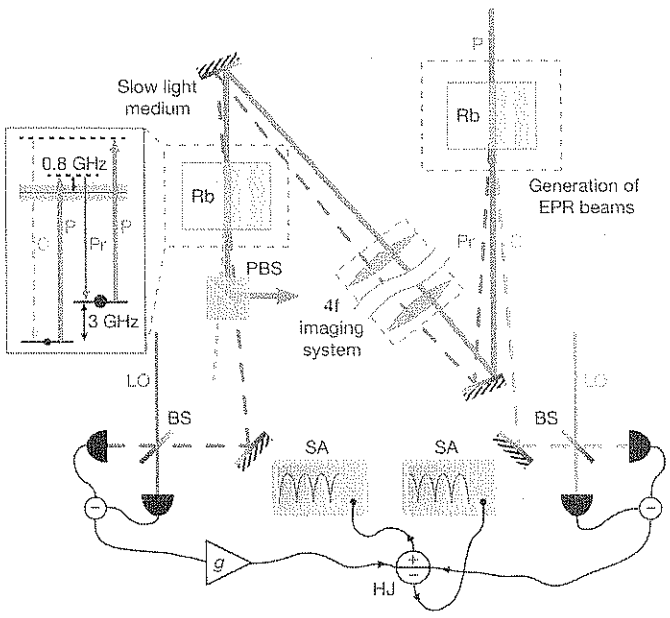

Figure 1 | Experimental set-up. In the first Rb cell (on the right), the four-wave mixing process is used to generate EPR entangled beams, which we call the probe (Pr) and the conjugate (C). The process is tuned to a gain $G \approx 4$ (at a temperature of 113 °C) and fed with vacuum states, so that vacuum twin beams are generated. After the first cell the conjugate is detected with a homodyne detector, while the probe and pump (P) are imaged with a 4f optical system into a second Rb cell. This second cell serves as the slow light medium for the probe, and is used to introduce a tunable delay between the probe and the conjugate generated by the first cell. After the second cell, the pump and the delayed probe are separated with a polarizing beam splitter (PBS) after which the probe is detected with a second homodyne detector. The sum and difference signals of the two homodyne detectors are obtained with a hybrid junction (HJ) and analysed with two spectrum analysers (SA). To obtain good spatial mode matching and phase stability when performing the homodyne detection, the local oscillators (LOs) are generated with a second four-wave mixing process in the first cell, as was done in ref. 19. The local oscillator for the probe follows a similar path as the probe through the slow light medium so that any spatial distortion is imparted to both beams. A variable electronic gain (g) is used to adjust the weighting of the homodyne detector signals in order to optimize the squeezing between the delayed probe and the conjugate. Both Rb cells have anti-reflection coated windows and are 12.5 mm long. Inset, energy level diagram for the four-wave mixing process in the D1 line of ^{85}Rb. BS, 50/50 beam splitter.

and then delay the entanglement, as shown in Fig. 1. In the first cell, entangled vacuum twin beams, called the probe and the conjugate, are generated. The second cell serves as the slow light medium for the probe, and introduces a tunable delay between the probe and the conjugate generated by the first cell. The delay can be controlled by changing the value and bandwidth of the gain, which can be done through changes in the temperature and pump power used for the four-wave mixing in the slow light cell.

Measurements of the amplitude and phase quadratures of the probe and conjugate require homodyning with local oscillators. In these measurements, the phase of the homodyne detector, or relative phase between the probe or conjugate and the corresponding local oscillator, determines the quadrature that is measured. Each beam is detected with a separate homodyne detector and the phases of the local oscillators are scanned synchronously, such that both homodyne detectors always have the same phase θ and measure the same quadrature[19], that is $\hat{X}^{\theta}_{(a,b)} = \hat{X}_{(a,b)} \cos\theta + \hat{Y}_{(a,b)} \sin\theta$. The results of both measurements are added and subtracted to obtain the joint quadratures, and the noise properties of the signals are then measured with a radio frequency spectrum analyser. The results obtained from these measurements are shown on the top row of Fig. 2 for different delays.

We use a variable electronic gain (g) in the homodyne detector for the delayed probe to adjust the weighting of the homodyne detector signals in order to optimize the squeezing measurements for the joint quadratures. This allows us to obtain the optimum value for the inseparability parameter $\mathcal{I}$. The conditional variances, required to evaluate the EPR parameter, for the conjugate given the probe can be obtained using g to optimize the squeezing with respect to the SQL of the conjugate alone[20]. In general, the values of g that minimize $\mathcal{I}$ and $\mathcal{E}_{ab}$ are not the same[21]. We can, however, use the data taken with g optimized for the inseparability parameter together with noise measurements of the individual beams to calculate the conditional variances for the EPR criterion, as described in the Supplementary Information.

The delay is characterized by the time shift in the cross-correlation function between the delayed probe and the conjugate with respect to the reference cross-correlation function, which is obtained when there is no four-wave mixing in the second cell. To calculate the correlation function of the entangled vacuum twin beams directly, we record the time traces of the photocurrents obtained from each of the homodyne detectors after filtering out the d.c. part. The correlation function has an oscillatory behaviour due to an offset of the local oscillator frequency with respect to the centre of the gain profile of the four-wave mixing process. We obtain the envelope of the correlation functions by taking data for different quadratures of the vacuum twin beams. Since the phases of the homodyne detectors are not actively stabilized, we acquire the time traces by triggering the data acquisition system at a given noise level of the signal measured by one of the spectrum analysers, which corresponds to a specific phase θ. This makes it possible to obtain data only when the homodyne detectors are measuring a specific combination of quadratures, that is, $\hat{X}^{\theta}_{(a,b)}$ (see Supplementary Information).

With our experimental parameters, the initial state is EPR entangled, with $\mathcal{E}_{ab} = 0.47(4) < 1$ and $\mathcal{I} = 0.72(3) < 2$ (Fig. 2a). As the delay is increased to 22 ns, for a fractional delay of 0.44, the squeezing in both joint quadratures is reduced to 3 dB, such that EPR entanglement is still present with $\mathcal{E}_{ab} = 0.71(9) < 1$ and $\mathcal{I} = 0.97(3) < 2$ (Fig. 2b). This point is significant, as some protocols, such as e-cloning[22], entanglement swapping[23], and teleportation of arbitrary coherent states[24], require at least 3 dB of squeezing in both joint quadratures. EPR entanglement is lost at a delay of 27 ns, as shown in Fig. 3, which corresponds to a fractional delay of 0.52. We finally increase the delay to 32 ns, for a fractional delay of 0.6. At this point a small amount of entanglement is still present, but only the inseparability criterion is satisfied with $\mathcal{I} = 1.74(3) < 2$ (Fig. 2c).

As shown in Fig. 3, longer delays require a larger gain in the slow light cell. This gain, associated with the four-wave mixing process that leads to a reduced group velocity, is the main source of excess noise responsible for the degradation of the entanglement. The gain is linked to the generation of a second conjugate which is quantum correlated with the delayed probe. As the second conjugate is not measured, this is equivalent to tracing the density matrix of the whole system over that beam, which leads to a mixed state and thus to excess noise on the delayed probe. Inseparability is more robust to sources of excess noise than EPR entanglement, as can be seen from Fig. 3, as it is independent of the purity of the state[21]. A gain of more than 2, as seen in Fig. 3, is possible while still satisfying the inseparability criterion.

The optical tunability of the system is illustrated by the fact that the delay disappears (blue correlation functions in Fig. 2) when the pump input to the slow light cell is blocked. When this is done the initial degree of entanglement is substantially recovered. As the temperature of the slow light cell is increased, absorption of the probe as it propagates through the cell increases and leads to a small degradation of the entanglement. In principle it is possible to combine both the temperature and pump power tuning capabilities of the system to obtain even larger delays. However, reducing the pump power makes the bandwidth over which a delay can be obtained smaller than the squeezing bandwidth of our initial state. This leads to distortion and break-up of the cross-correlation function and makes it hard to characterize the delay with our current experimental

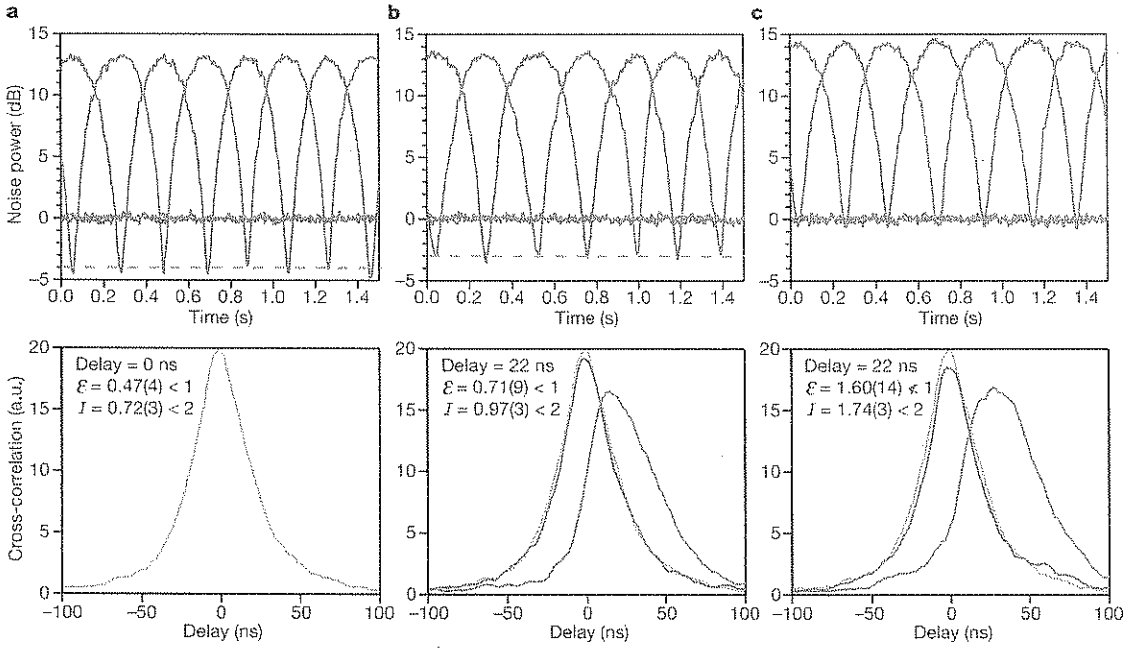

Figure 2 | Delay of EPR entanglement. Top row, the entanglement is characterized by measuring the noise power of the sum (red curves) and difference (blue curves) signals of the homodyne detectors as the phase θ is scanned. These measurements are done for a slow light cell temperature of 23 °C (**a**), 91 °C (**b**) and 100 °C (**c**). The minima of the blue and red curves give the variance of the intensity difference ($\langle \Delta \hat{X}_-^2 \rangle$) and phase sum ($\langle \Delta \hat{Y}_+^2 \rangle$), respectively, needed to calculate the entanglement criteria. The relative delay between the probe and conjugate is characterized by measuring the cross-correlation between their fluctuations. Bottom row, the envelopes of the cross-correlation functions for the corresponding temperatures of the slow light cell. The grey curve shows the correlation function that is obtained when there is no four-wave mixing in the slow light cell and is taken as the reference cross-correlation function for the delay measurements. This effectively corresponds to the output from the first cell. The red curves give the cross-correlation between the delayed probe and the conjugate. The delay can be controlled by changing the temperature or the pump power in the slow light cell. The blue curves show the cross-correlation functions when the pump beam for the slow light cell is blocked, which illustrates the optical tuning capabilities of the system. The envelopes of the correlation functions are calculated by taking data for 10 different phases of the homodyne detectors evenly distributed between 0 and $\pi/2$ (discussed in detail in the Supplementary Information). A data acquisition system with a rate of 1 GHz is used to record 50 time traces with 10,000 points for each trigger level, whose correlation functions are averaged. The numbers in parenthesis are combined statistical and systematic uncertainties estimated at one standard deviation. a.u., arbitrary units.

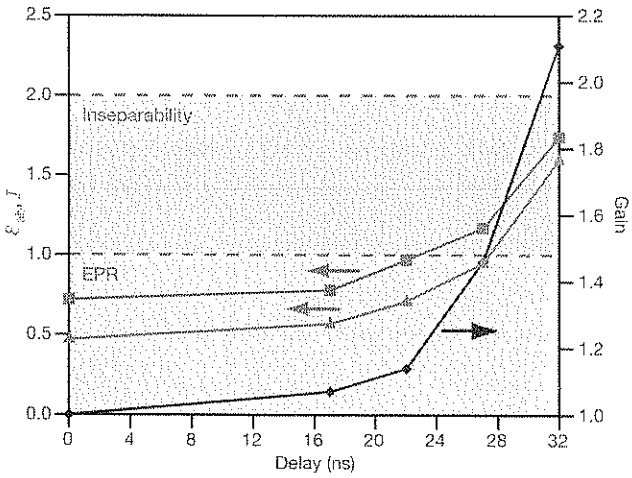

Figure 3 | Effect of the gain in the slow light cell on the quantum correlations. The black curve shows the gain in the slow light cell as a function of the delay of the probe. The red curve shows $\mathcal{E}_{ab}$ as a function of the delay. $\mathcal{E}_{ab} < 1$ (indicated by the red shaded region) indicates the presence of EPR entanglement. The blue curve shows $\mathcal{I}$ as a function of the delay. $\mathcal{I} < 2$ (indicated by the blue plus red shaded regions) indicates inseparability between the delayed probe and the conjugate. EPR entanglement is lost for a delay of about 27 ns, which corresponds to a gain of about 1.5. The inseparability is more robust to sources of excess noise, and is still present for a delay greater than 32 ns and a gain larger than 2. Longer delays require larger gains in the slow light cell, as can be seen from the black curve. This increase in gain leads to a quick deterioration of the quantum correlations.

set-up. Optical control of the delay would, however, allow for fast tuning of the propagation speed of the quantum correlated light.

The delays obtained with the four-wave mixing represent an important step towards achieving a fractional delay larger than one while maintaining the entanglement levels needed for quantum protocols in general. Even though gain degrades the quantum correlations, it should be possible to increase the fractional delay by, for example, modifying the gain profile to optimize the dispersive properties of the medium[25]. In addition, it has been recently shown that four-wave mixing in the double-lambda configuration can be used for storage in the classical regime[26]. In principle, it should be possible to use our system for the storage of quantum states.

Recently, there has been interest in extending the storage properties of quantum memories to include the transverse spatial information of the beams of light, such that the propagation of images can be controlled. Up to now, the results on this front have been limited to the delay and storage of classical images[26,27]. An important property of the four-wave mixing process used here is that it supports multiple spatial modes. This has important consequences in the generation of entangled beams of light, as it allows for subregions of the beams to be independently correlated[28] or entangled and makes it possible to obtain entanglement between complicated spatial patterns, that is, entangled images[19]. Each of the spatial modes supported by the four-wave mixing will experience gain and thus a delay. We illustrate this property by showing the delay of a particular entangled image with the shape of the '$\hbar$' symbol, as shown in Fig. 4. We have obtained a tunable relative delay between the entangled multi-spatial-mode probe and conjugate beams of up to 27 ns, for a fractional delay of 0.45, while still preserving the inseparability of the images. As a result

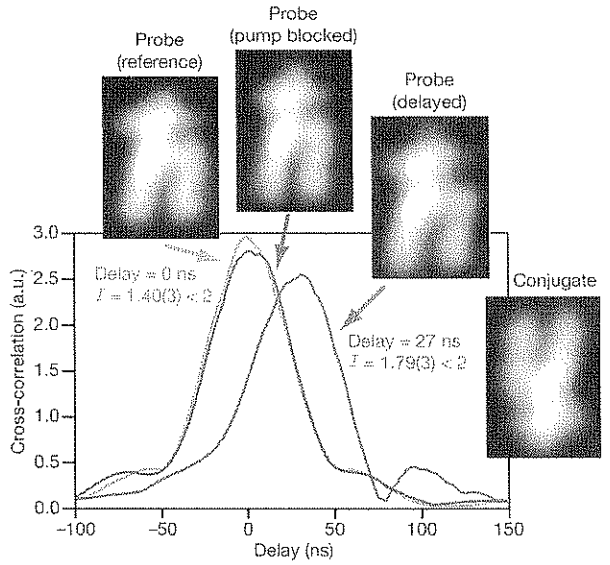

Figure 4 | Delay of an entangled image of the '*h*' symbol. The four-wave mixing process preserves the spatial quantum correlations, such that for entangled images we can obtain a tunable relative delay of up to 27 ns between the probe and the conjugate. This corresponds to a fractional delay (ratio of the delay to the width of the correlation function) of 0.45. The spatial pattern for the conjugate is shown on the right side of the figure. The grey curve shows the cross-correlation between probe and conjugate when there is no delay, that is, the reference cross-correlation function. The red curve shows the cross-correlation function at the point where only a small degree of entanglement, $\mathcal{I} = 1.79(3) < 2$, is left between the delayed probe and the conjugate. The blue curve shows the cross-correlation function when the pump for the slow light cell is blocked, showing the optical tunability of the system. The four-wave mixing in the second cell introduces a slight distortion on the probe due to a cross-Kerr effect with the pump. In homodyne detection the shape of the local oscillator acts as a spatial filter that selects the spatial mode that is measured for the probe and conjugate, so that quantum correlations between arbitrary spatial modes can be characterized through the proper choice of local oscillators[19]. The images shown here correspond to the '*h*' shaped local oscillators (also generated by four-wave mixing [19]) that are used to measure the entanglement of vacuum twin beams in an '*h*' mode. a.u., arbitrary units.

of the phase-matching condition, given by the conservation of momentum, different spatial modes experience different gains and thus different delays. This leads to a slight broadening and distortion of the cross-correlation function.

We have demonstrated that four-wave mixing makes it possible to obtain a tunable delay of EPR entangled beams of light with a fractional delay of up to 0.52. This is a step towards applications such as distributed quantum computation, protocols based on teleportation of arbitrary quantum states, entanglement swapping, and so on. The ability to delay entangled images makes it possible to extend the intrinsic parallelism of image processing to the quantum regime. In addition, the capability of supporting multiple spatial modes offers advantages in terms of speed and reliability for quantum communication[29] and computing[30] schemes. The dependence of the delay on the pump power, combined with the spatial properties of the system, offer the possibility of using the spatial profile of the pump to independently control the delay of different spatial modes. For example, having a pump beam smaller than the probe in the cell would only introduce a delay on the overlapping regions. This would make it possible to control the transfer of a large amount of quantum resources in parallel.

Received 28 October; accepted 22 December 2008.

1. Galindo, A. & Martin-Delgado, M. A. Information and computation: Classical and quantum aspects. *Rev. Mod. Phys.* 74, 347–423 (2002).
2. Braunstein, S. L. & van Loock, P. Quantum information with continuous variables. *Rev. Mod. Phys.* 77, 513–577 (2005).
3. Kimble, H. J. The quantum internet. *Nature* 453, 1023–1030 (2008).
4. Vasilyev, D. V., Sokolov, I. V. & Polzik, E. S. Quantum memory for images: A quantum hologram. *Phys. Rev. A* 77, 020302(R) (2008).
5. Hau, L. V., Harris, S. E., Dutton, Z. & Behroozi, C. H. Light speed reduction to 17 metres per second in an ultracold atomic gas. *Nature* 397, 594–598 (1999).
6. Camacho, R. M., Pack, M. V., Howell, J. C., Schweinsberg, A. & Boyd, R. W. Wide-bandwidth, tunable, multiple-pulse-width optical delays using slow light in cesium vapor. *Phys. Rev. Lett.* 98, 153601 (2007).
7. Boyer, V., McCormick, C. F., Arimondo, E. & Lett, P. D. Ultraslow propagation of matched pulses by four-wave mixing in an atomic vapor. *Phys. Rev. Lett.* 99, 143601 (2007).
8. Broadbent, C. J., Camacho, R. M., Xin, R. & Howell, J. C. Preservation of energy-time entanglement in a slow light medium. *Phys. Rev. Lett.* 100, 133602 (2008).
9. Chanelière, T. *et al.* Storage and retrieval of single photons transmitted between remote quantum memories. *Nature* 438, 833–836 (2005).
10. Eisaman, M. D. *et al.* Electromagnetically induced transparency with tunable single-photon pulses. *Nature* 438, 837–841 (2005).
11. Choi, K. S., Deng, H., Laurat, J. & Kimble, H. J. Mapping photonic entanglement into and out of a quantum memory. *Nature* 452, 67–71 (2008).
12. Akamatsu, D. *et al.* Ultraslow propagation of squeezed vacuum pulses with electromagnetically induced transparency. *Phys. Rev. Lett.* 99, 153602 (2007).
13. Honda, K. *et al.* Storage and retrieval of a squeezed vacuum. *Phys. Rev. Lett.* 100, 093601 (2008).
14. Appel, J., Figueroa, E., Korystov, D., Lobino, M. & Lvovsky, A. I. Quantum memory for squeezed light. *Phys. Rev. Lett.* 100, 093602 (2008).
15. Hétet, G. *et al.* Delay of squeezing and entanglement using electromagnetically induced transparency in a vapour cell. *Opt. Express* 16, 7369–7381 (2008).
16. Duan, L. M., Giedke, G., Cirac, J. I. & Zoller, P. Inseparability criterion for continuous variable systems. *Phys. Rev. Lett.* 84, 2722–2725 (2000).
17. Reid, M. D. Demonstration of the Einstein-Podolsky-Rosen paradox using nondegenerate parametric amplification. *Phys. Rev. A* 40, 913–923 (1989).
18. McCormick, C. F., Marino, A. M., Boyer, V. & Lett, P. D. Strong low-frequency quantum correlations from a four-wave-mixing amplifier. *Phys. Rev. A* 78, 043816 (2008).
19. Boyer, V., Marino, A. M., Pooser, R. C. & Lett, P. D. Entangled images from four-wave mixing. *Science* 321, 544–547 (2008).
20. Ou, Z. Y., Pereira, S. F., Kimble, H. J. & Peng, K. C. Realization of the Einstein-Podolsky-Rosen paradox for continuous-variables. *Phys. Rev. Lett.* 68, 3663–3666 (1992).
21. Bowen, W. P., Schnabel, R., Lam, P. K. & Ralph, T. C. Experimental characterization of continuous-variable entanglement. *Phys. Rev. A* 69, 012304 (2004).
22. Weedbrook, C., Grosse, N. B., Symul, T., Lam, P. K. & Ralph, T. C. Quantum cloning of continuous-variable entangled states. *Phys. Rev. A* 77, 052313 (2008).
23. Tan, S. M. Confirming entanglement in continuous variable quantum teleportation. *Phys. Rev. A* 60, 2752–2758 (1999).
24. Grosshans, F. & Grangier, P. Quantum cloning and teleportation criteria for continuous quantum variables. *Phys. Rev. A* 64, 010301(R) (2001).
25. Boyd, R. W., Gauthier, D. J., Gaeta, A. L. & Willner, A. E. Maximum time delay achievable on propagation through a slow-light medium. *Phys. Rev. A* 71, 023801 (2005).
26. Vudyasetu, P. K., Camacho, R. M. & Howell, J. C. Storage and retrieval of multimode transverse images in hot atomic rubidium vapor. *Phys. Rev. Lett.* 100, 123903 (2008).
27. Shuker, M., Firstenberg, O., Pugatch, R., Ron, A. & Davidson, N. Storing images in warm atomic vapor. *Phys. Rev. Lett.* 100, 223601 (2008).
28. Boyer, V., Marino, A. M. & Lett, P. D. Generation of spatially broadband twin beams for quantum imaging. *Phys. Rev. Lett.* 100, 143601 (2008).
29. Collins, O. A., Jenkins, S. D., Kuzmich, A. & Kennedy, T. A. B. Multiplexed memory insensitive quantum repeaters. *Phys. Rev. Lett.* 98, 060502 (2007).
30. Tordrup, K., Negretti, A. & Molmer, K. Holographic quantum computing. *Phys. Rev. Lett.* 101, 040501 (2008).

Supplementary Information is linked to the online version of the paper at www.nature.com/nature.

Acknowledgements R.C.P. is supported by the Intelligence Community Postdoctoral Program.

Author Information Reprints and permissions information is available at www.nature.com/reprints. Correspondence and requests for materials should be addressed to A.M.M. (alberto.marino@nist.gov).